

Kinetic Modeling of Precipitation and Dispersion Polymerizations



L. Ivano Costa and G. Storti

Abstract Dispersion and precipitation polymerizations represent a simple and attractive synthetic platform for the production of a large variety of polymers and micron-sized particles. Although the main qualitative features of these processes have been known for a long time, obtaining quantitative descriptions of the polymerization kinetics and, especially, the full molecular weight distributions, is still a major challenge because of the heterogeneous nature of the reactions. This review summarizes the most relevant aspects of the processes involved, focusing on the free-radical polymerization mechanism, with special emphasis on the key role of radical interphase transport. We describe a unified mathematical modeling framework that has enabled accurate description of reaction rates and evolution of molecular weight distributions in a number of cases. Examples of copolymerization reactions carried out in organic and supercritical fluids are discussed to demonstrate the reliability and capabilities of the modeling approach.

Keywords Diffusion • Dispersed systems • Dispersion polymerization • Modeling • Precipitation polymerization • Radical polymerization

Contents

1	Introduction	46
2	Mechanism of Reaction and Polymerization Locus	49
3	Model Framework	52
	3.1 Key Assumptions	52

L.I. Costa
Etzbergstrasse 19c, 8405 Winterthur, Switzerland
e-mail: liborio78@gmail.com

G. Storti (✉)
Institute for Chemical and Bioengineering, ETH Zürich, Vladimir-Prelog-Weg 1-5/10, 8093
Zürich, Switzerland
e-mail: giuseppe.storti@chem.ethz.ch

3.2	Material and Population Balance Equations	53
3.3	Kinetic Rate Constants	56
3.4	Transport Parameters	58
4	Applications	61
4.1	Precipitation Polymerization in Organic Solvent	61
4.2	Precipitation and Dispersion Copolymerizations in Supercritical Carbon Dioxide ..	65
4.3	Precipitation Polymerization of Vinyl Chloride	69
5	Conclusions	72
	References	73

1 Introduction

Dispersion polymerization is a heterogeneous polymerization process enabling the production of micron-sized polymer particles with narrow size distributions [1–3]. Even though different polymerization mechanisms can be applied [4], free-radical polymerization is by far the most popular and it is the only one considered here. Dispersion polymerization can be considered an evolution of precipitation polymerization. In precipitation polymerization, the initial system is a homogeneous solution of monomer and initiator in a solvent in which the polymer is insoluble. As the polymerization proceeds, the system undergoes phase separation. The polymer chains nucleate first in the form of unstable nuclei, which then aggregate and/or coalesce to eventually form large polymer aggregates, as sketched in Fig. 1. In dispersion polymerization, a suitable stabilizer (or simply “surfactant”) is initially added to the system. The stabilizer adsorbs or anchors to the surface of the polymer particles and hinders their aggregation/coalescence, thus leading to a stable colloidal dispersion. Ionic, nonionic, steric, and polymeric stabilizers can be used, the choice depending on the nature of the system [1–5].

In precipitation polymerization, the irregular aggregates produced in the absence of surfactant have sizes in the range 1–100 μm . In dispersion polymerization, roughly spherical particles of 0.1–10 μm are formed in the presence of sufficient effective surfactant. In both cases, the polymerization occurs under heterogeneous conditions in the presence of a continuous solvent-rich phase and a dispersed monomer-swollen and polymer-rich phase. For this reason, we refer to such systems in general as “dispersed systems”, even when dealing with precipitations.

Dispersion polymerization was initially developed with the aim of producing coating formulations with high polymer content and low viscosity, and many of the early reports on dispersion polymerizations are in fact patents from the chemical industry for such applications [6–9]. For the same reason, most early studies focused on reactions carried out in nonpolar organic solvents such as low molecular weight hydrocarbons, which, being highly volatile, are ideal candidates for coating formulations [10, 11]. Nevertheless, this technique is not limited to the use of nonpolar solvents, and reactions carried out in polar solvents have been reported since the 1980s [2, 3, 5]. The range of suitable solvents was further extended to the use of nonconventional solvents such as supercritical carbon dioxide (scCO_2) with

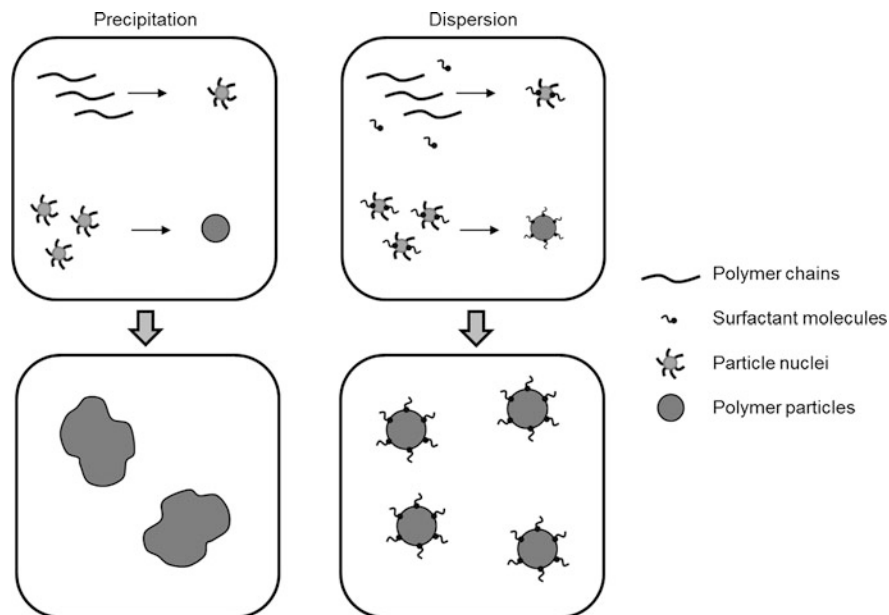


Fig. 1 Time evolution of precipitation/dispersion free-radical polymerization processes. *Top*: Starting from a single homogenous phase, insoluble polymer chains are formed, which nucleate in unstable particle nuclei that aggregate/coalesce into polymer particles. *Bottom*: Without surfactant (precipitation), large irregularly shaped particles are formed; with surfactant (dispersion), smaller more regular particles are produced

the aim of replacing the more typical, but often hazardous and/or toxic, organic solvents [12]. Because many common low molecular weight monomers are easily soluble in scCO_2 , but most high molecular weight polymers are not [13, 14], heterogeneous polymerizations in scCO_2 under precipitation or dispersion conditions are relatively straightforward to accomplish, at least on a laboratory scale [15–24].

More recently, it has been realized that precipitation and dispersion polymerizations are relatively simple and effective techniques for production of micron-sized particles with advanced structures and functionalities. Extensive and updated reviews cover this topic; for example, Li et al. [25] and Pich and Richtering [26] report the use of precipitation polymerization for the preparation of hollow structures and aqueous microgels, while Zhang [27] and Sun et al. [28] review the emerging field of controlled heterogeneous polymerization techniques for the synthesis of “living” functionalizable nano-objects and supramolecular objects ranging from micelles to vesicles and worms. Thus, although precipitations and dispersions are mature techniques for the production of a large variety of polymers and colloidal microspheres for conventional applications, at the same time they represent a simple and versatile platform for the synthesis of advanced nanomaterials.

Compared with the large amount of experimental activity in the field [4], the number of works that focus on quantitative modeling of polymerization kinetics in dispersed systems is relatively low. The reason for this can be attributed to the complexity of such systems when reliable quantification of the physical and chemical phenomena involved is required. As mentioned above, a fully detailed kinetic description requires the modeling of particle nucleation and of surfactant partitioning between the phases, which in turn dictates the final number of particles and their stability behavior (i.e., the rate at which they aggregate). In parallel, the monomer often swells the polymer particles and, hence, the polymerization reaction may occur in both the continuous and dispersed phases, making the identification of the predominant locus of polymerization a nontrivial task [24, 29–31]. This is due to the fact that the relative contribution of the polymerization rate in the two phases is affected by many system parameters, as Jiang et al. [32] and Saenz and Asua [33] have shown through their experimental investigation of the kinetics of dispersion homopolymerization of methyl methacrylate in methanol/water mixtures, and of dispersion copolymerization of styrene and butyl acrylate in ethanol/water.

In view of this complexity, the first proposed kinetic models for dispersed systems were quite empirical and aimed to describe reaction rate and average molecular weight, rather than the full polymer molecular weight distribution (MWD) or aspects related to particle nucleation and particle size distribution. In this respect, the works of Barrett and Thomas on the dispersion polymerization of methyl methacrylate [10], of Crosato-Arnaldi et al. and Olay on the heterogeneous polymerization of vinyl chloride [34, 35], and of Avela et al. on the precipitation polymerization of acrylic acid [36] deserve special mention. One of the first attempts to model the full MWD was made by Abdel-Alim and Hamielec [37] and was followed by more comprehensive, two-phase models [38–45]. It was realized that the radical interphase transport between the continuous and dispersed phases is one of the most crucial aspects for reliable modeling of precipitations and dispersions [43–45]. By properly accounting for such transport process, a common modeling framework was developed for these complex processes and found to be successful in modeling both homopolymerizations [43–46] and copolymerizations [47, 48].

It is the aim of this contribution to review such modeling framework that enables the prediction of reaction rates and MWDs for this type of heterogeneous polymerizations. The model accounts for all the most relevant reactions taking place in both phases (continuous and dispersed) as well as for the partitioning of the different species between the phases. Namely, while all low molecular weight species are assumed to be partitioned according to thermodynamic equilibrium, the transport rate of active chains (or radicals) is accounted for explicitly as the key factor determining the relative contribution of each phase to the polymer buildup (i.e., as reaction locus). Notably, the model does not include population balances for the particle size distribution of the dispersed phase, thus relying on simpler, ordinary differential equations. The only particle-related property needed as model input is the total interphase surface area. Different approaches have been suggested for its reliable evaluation, depending upon particle morphology or experimentally

observable parameters, without relying on complex particle population balances that require inclusion of additional mechanisms (e.g., particle nucleation and aggregation/breakage terms) into the model [38–40, 49, 50]. Once a model for the specific system under examination has been validated and all parameters evaluated, the (particle) population balances can be integrated into the model equations if information about the particle size distribution are of relevance. This separation between kinetics and particle size distribution is convenient for facilitating an understanding of the mechanistic behavior of the system and improving the reliability of the estimated model parameters.

The polymerization mechanism is discussed in Sect. 2 and the possible operating regimes are rationalized in terms of dimensionless quantities correlating transport properties and termination rates. In Sect. 3, the main model equations are presented and suitable strategies and correlations for evaluating the parameters are provided. In Sect. 4, three case studies illustrate the capabilities of the proposed modeling approach in predicting conversion and evolution of MWD.

2 Mechanism of Reaction and Polymerization Locus

The polymerization starts in a single-phase, homogeneous system (the solvent-rich phase). Accordingly, in the early stages of polymerization, all the kinetic steps typical of free-radical polymerization (initiation, propagation, and terminations) occur in this phase, as schematically shown in Fig. 1. However, as soon as insoluble polymer chains are formed, they phase-separate and aggregate into unstable primary nuclei, which eventually coalesce into stable particles. From this moment on, the system becomes heterogeneous and two phases are present: the continuous, solvent-rich phase and the newly formed dispersed, polymer-rich phase. The generation of polymer particles proceeds until the overall surface area of the polymer phase is so large that all polymer chains formed in the continuous phase are “captured” by the particles; that is, the process of diffusion into existing particles becomes much faster than their aggregation into primary nuclei [1, 49, 51]. When present, surfactant molecules absorb or anchor on the surface of the particles and prevent further coalescence and/or aggregation.

Experimental and theoretical evidences indicate that the nucleation phase generally occurs in the first few seconds to minutes of the reaction and is already complete after few percent of monomer conversion [49, 52–54]. Subsequently, the concentration of particles remains constant provided that an effective surfactant is present in the system. When the surfactant is not effective enough or absent (as in precipitation polymerization), polymer particles may coalesce and/or aggregate, which leads to a decrease in their concentration. This can result in a longer nucleation phase, because capture by pre-formed particles is less efficient in view of the reduced overall surface area.

As already mentioned, once the system evolves from homogeneous to heterogeneous, the reaction proceeds in both phases provided that the monomer is at least partly solubilized in the dispersed phase. Identification of the relative contribution

of the reaction in each phase is crucial for reliable prediction of the evolution of polymer buildup. The relevance of each reaction locus can be conveniently rationalized in terms of the dimensionless “second Damköhler number,” or equivalently from its reciprocal, the so-called Ω parameter [45, 55]. Let us assume that, at a given instant in time, the total volumes of the continuous and dispersed phases are V_1 and V_2 , respectively, and that the total interphase area (i.e. the total particle surface area) is A_p . For each phase j the quantity Ω_j is defined as the ratio between the rate of diffusion of radicals from that phase to the other phase and the rate of termination of the radicals in the same phase j :

$$\Omega_1 = \frac{KA_p}{V_1 k_{t,1} [R_1]} \quad (1)$$

$$\Omega_2 = \frac{\alpha KA_p}{V_2 k_{t,2} [R_2]} \quad (2)$$

where K is the overall mass transfer coefficient for phase 1, $[R_j]$ is the overall concentration of active chains in phase j and α is the partition coefficient of the radicals between the two phases at thermodynamic equilibrium:

$$\alpha = \frac{[R_1]_{\text{eq}}}{[R_2]_{\text{eq}}} \quad (3)$$

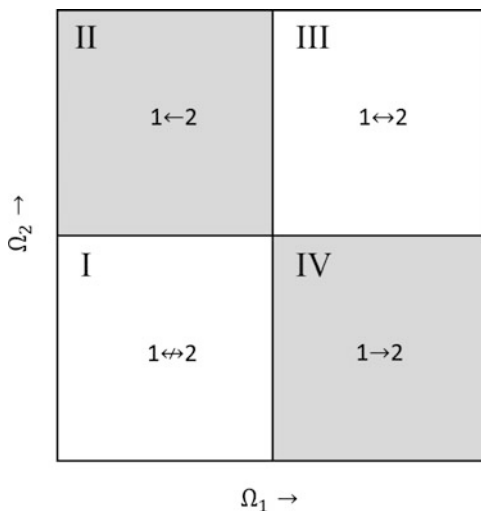
where $[R_j]_{\text{eq}}$ indicates the equilibrium concentration of active chains in phase j .

In general, parameters such as α , $k_{t,j}$, and K are dependent on composition and chain length and, therefore, Ω_j is also dependent on these parameters (a detailed discussion about their meaning and evaluation is provided in the following sections). However, for the sake of simplicity, let us neglect such dependencies here and assume constant Ω_j values. According to Eqs. 1 and 2, a value of Ω_j much larger than 1 means that the rate at which radicals in phase j diffuse out of that phase is much larger than the rate at which they terminate in the same phase. On the other hand, the opposite is true when Ω_j is much smaller than 1 (i.e., the rate of termination of the radicals in phase j is much larger than the rate at which they diffuse to the other phase). It follows that four limiting operating regimes can be readily identified according to the Ω values, as represented in the master plot in Fig. 2:

(I) $\Omega_1 \ll 1$ and $\Omega_2 \ll 1$: The termination rate is higher than that of diffusion out for both phases. This implies that radicals predominantly terminate in their original phase and the system can be considered segregated with respect to radical partitioning, in view of their limited transfer from one phase to the other.

(II) $\Omega_1 \ll 1$ and $\Omega_2 \gg 1$: The termination rate is higher than that of diffusion out only for the continuous phase, whereas the opposite is true for the dispersed phase. Accordingly, radicals generated in the dispersed phase diffuse out and eventually terminate in phase 1 (from where they cannot diffuse out because $\Omega_1 \ll 1$), and the continuous phase is the main reaction locus.

Fig. 2 Ω Master plot showing the four operating regions in terms of radical distribution: *I* segregated system, *II* phase 1 favored, *III* equilibrated distribution, and *IV* phase 2 favored



(III) $\Omega_1 \gg 1$ and $\Omega_2 \gg 1$: The rate of diffusion out of one phase is larger than the termination rate for both phases. Therefore, radicals are exchanged between the two phases very rapidly and, on average, each radical crosses the boundary from one phase to the other many times before terminating in one of the two phases. Under such conditions, the radicals achieve thermodynamic equilibrium between the two phases.

(IV) $\Omega_1 \gg 1$ and $\Omega_2 \ll 1$: This case is the opposite of case II. Radicals generated in the continuous phase ($j=1$) diffuse to the dispersed phase ($j=2$) much faster than they terminate in their original phase. By contrast, radicals in the dispersed phase terminate there before diffusing out to the continuous phase. Irrespective of where the radicals are generated, they predominantly terminate in the dispersed phase, which therefore represents the main reaction locus.

The four sectors in Fig. 2 correspond to the four operating regions identified above. Given the Ω values for each phase, the location of a given system in this plane can be found and the corresponding picture in terms of radical interphase transport readily assessed, from which the predominant reaction locus (if any) can be quickly identified. On the other hand, even if very short oligomers are partly soluble in the continuous phase, the continuous phase is a poor solvent for the polymer and the partition coefficient is expected to decay rapidly as the length of the chains increases. Therefore, because the partition coefficient α is usually very small, the case $\Omega_2 \ll 1$ occurs frequently. This means that the operating conditions for dispersed systems are determined by the value of Ω_1 alone, and regimes I and IV are the only feasible limiting regimes.

Given the key relevance of the Ω value of the continuous phase, the next question is how to control its value and, therefore, how to determine the operating regime of a given polymerization system. Because reaction rate constants and transport coefficients are given once the specific chemistry of a system is selected,

the most relevant tunable parameter is the interphase area, A_p . Specifically, a system is radical-segregated for extremely low values of the particle surface area, whereas the dispersed phase is the dominant reaction locus for very large values. Accordingly, this particle property becomes very important in determining not only the particle size and colloidal stability, which is expected, but also the two main aspects of the overall polymerization kinetics, reaction rate, and MWD. This interplay is described in more detail in the following sections.

3 Model Framework

In this section, the main constitutive model equations, as well as the correlations required to estimate the most relevant parameters, are reported and discussed. For the sake of clarity, the equations are written for a single monomer case (homopolymerization) and a basic radical polymerization scheme, but the same approach can be easily extended to the case of multiple monomers and more complex kinetic schemes, including chain transfer and crosslinking reactions [43, 45, 47, 48].

3.1 Key Assumptions

According to the phenomenological picture described above, the following key assumptions are considered:

- (1) Particle nucleation is instantaneous and not accounted for in the model. As previously noted, this assumption is justified by the observation that the nucleation period in dispersion polymerization systems is much shorter than the overall polymerization time [49, 53, 54, 56]. Therefore, the role of the stabilizer in determining the particle concentration is not explicitly considered and a constant number of polymer particles (small enough to correspond to a negligible polymer amount at the end of the nucleation phase) is assumed to be present since the early phase of the reaction. This assumption is also considered valid for the case of precipitation polymerization. From a practical viewpoint, this implies that, in the absence of seeds (pre-formed particles), one can consider the system as homogeneous until a critical percentage conversion, X_{cr} , is reached. At $X = X_{cr}$, polymer particles form instantaneously and the reaction proceeds under heterogeneous conditions with a constant particle concentration. The value of X_{cr} is typically below 1%. The corresponding initial value of the particle size is readily evaluated given the particle number.
- (2) Low molecular weight species (solvent, initiator, monomer) are in thermodynamic equilibrium between the continuous solvent-rich phase and the dispersed

Table 1 Kinetic scheme

Reaction step	Reaction scheme	Rate [mol L ⁻¹ s ⁻¹]
Initiation	$I_j \xrightarrow{k_{d,j}} 2I_j^*$	$k_{d,j}I_j$
	$I_j^* + M_j \xrightarrow{k_{I,j}} R_{1,j}^*$	$2f_j k_{d,j} I_j$ (for $k_{I,j} \gg k_{d,j}$)
Propagation	$R_{n,j}^* + M_j \xrightarrow{k_{p,j}} R_{n+1,j}^*$	$k_{p,j} R_{n,j}^* M_j$
Termination	$R_{n,j}^* + R_{m,j}^* \xrightarrow{k_{tc,j}} P_{n+m,j}$	$k_{tc,j} R_{n,j}^* R_{m,j}^*$
	$R_{n,j}^* + R_{m,j}^* \xrightarrow{k_{td,j}} P_{n,j} + P_{m,j}$	$k_{td,j} R_{n,j}^* R_{m,j}^*$
Interphase transport	$R_{n,1}^* \rightleftharpoons R_{n,2}^*$	$\frac{K_n A_p}{V_j} ([R_{n,1}^*] - \alpha_n [R_{n,2}^*])$

Where I_j , M_j , $R_{n,j}^*$, and $P_{n,j}$ represent initiator, monomer, and active and terminated polymer chains of length n in phase j , respectively

polymer-rich phase. Their partitioning is independent of particle size and there are no concentration gradients within the particles.

- (3) Both phases are considered as potential reaction loci (for $X > X_{cr}$), and the interphase mass transfer for the radicals is accounted for explicitly. The polymer particles are considered as a single pseudo-phase with homogeneous radical concentration.
- (4) Dead polymer is fully insoluble in the continuous phase and is considered instantaneously accumulated in the dispersed phase.

Given these general premises, the mathematical framework required to evaluate the system kinetics is detailed in the following subsections, with reference to the basic free-radical polymerization kinetic scheme detailed in Table 1. Note that the rate of radical diffusion between the two phases is also included in Table 1.

3.2 Material and Population Balance Equations

The mass balances for low molecular weight species and population balances for active and dead polymer chains are reported below. Subscripts 1 and 2 indicate continuous and dispersed phases, respectively, and the rates of all the kinetic events listed in Table 1 are considered.

$$\frac{dS}{dt} = 0 \quad (4)$$

$$\frac{dI}{dt} = -k_{d,1}[I_1]V_1 - k_{d,2}[I_2]V_2 \quad (5)$$

$$\begin{aligned} \frac{dM}{dt} = & -2f_1k_{d,1}[I_1]V_1 - 2f_2k_{d,2}[I_2]V_2 - k_{p,1}[M_1]V_1 \sum_{n=1}^{\infty} [R_{n,1}^*] \\ & - k_{p,2}[M_2]V_2 \sum_{n=1}^{\infty} [R_{n,2}^*] \end{aligned} \quad (6)$$

$$\begin{aligned} \frac{dR_{n,1}^*}{dt} = & \delta_{(n,1)}2f_1k_{d,1}[I_1]V_1 + k_{p,1}[M_1]V_1([R_{n-1,1}^*](1 - \delta_{(n,1)}) - [R_{n,1}^*]) + \\ & - [R_{n,1}^*]V_1 \sum_{m=1}^{\infty} (k_{tc,1} + k_{td,1})[R_{m,1}^*] - K_nA_p([R_{n,1}^*] - \alpha_n[R_{n,2}^*]) \end{aligned} \quad (7)$$

$$\begin{aligned} \frac{dR_{n,2}^*}{dt} = & \delta_{(n,1)}2f_2k_{d,2}[I_2]V_2 + k_{p,2}[M_2]V_2([R_{n-1,2}^*](1 - \delta_{(n,1)}) - [R_{n,2}^*]) + \\ & - [R_{n,2}^*]V_2 \sum_{m=1}^{\infty} (k_{tc,2} + k_{td,2})[R_{m,2}^*] + K_nA_p([R_{n,1}^*] - \alpha_n[R_{n,2}^*]) \end{aligned} \quad (8)$$

$$\frac{dP_{n,1}}{dt} = \frac{1}{2}V_1 \sum_{m=1}^{n-1} k_{tc,1}[R_{m,1}^*][R_{n-m,1}^*] + V_1[R_{n,1}^*] \sum_{m=1}^{\infty} k_{td,1}[R_{m,1}^*] \quad (9)$$

$$\frac{dP_{n,2}}{dt} = \frac{1}{2}V_2 \sum_{m=1}^{n-1} k_{tc,1}[R_{m,2}^*][R_{n-m,2}^*] + V_2[R_{n,2}^*] \sum_{m=1}^{\infty} k_{td,2}[R_{m,2}^*] \quad (10)$$

where f_j is the initiator efficiency, V_j the volume of phase j , K_nA_p the product of an overall radical transport coefficient and the total surface area of the particles, α_n the chain-length dependent partition coefficient for the radicals, and $\delta_{(n,1)}$ the delta Dirac function, which is equal to 1 when $n = 1$ and equal to 0 otherwise. While Eqs. 4–6 are written in terms of total number of moles of solvent, initiator, and monomer (S , I , and M) in both phases, the population balance equations (Eqs. 7–10) are the phase-specific, standard equations for free-radical polymerization systems. The only notable difference is the presence of the radical interphase transport (last term in Eqs. 7 and 8), which provides a coupling between the radical concentrations in the two phases. Note that the radical transport rate is expressed using the two-film theory [57] as the product of an overall transport coefficient and a driving force evaluated as the difference between the radical concentration in the continuous phase and the one in the same phase in equilibrium with the particle phase.

From the solution of the population balance equations, the moments of the first, leading orders of the polymer chain length distribution can be readily evaluated (e.g., $\lambda_i = \sum_{n=1}^{\infty} n^i(P_{n,1} + P_{n,2})$ for the i th order). Given the moments, calculation of the main average molecular weights follows from their definition. The overall mass of produced polymer, m , assumed to be completely in phase 2 (assumption 4) is readily evaluated as $m = \lambda_1 MW$, where MW is the molecular mass of the monomer repeating units.

To solve Eqs. 4–10, additional equations are needed to characterize the equilibrium partitioning of the low molecular weight species. At each instant of time, given the total amounts of solvent, initiator, monomer, and polymer (as calculated from Eqs. 4–10), the following equalities apply:

$$S = [S_1]V_1 + [S_2]V_2 \quad (11)$$

$$I = [I_1]V_1 + [I_2]V_2 \quad (12)$$

$$M = [M_1]V_1 + [M_2]V_2 \quad (13)$$

Moreover, the concentrations of solvent, initiator, and monomer in the two phases at equilibrium are constrained by the equality of the chemical potentials in the two phases:

$$\mu_{S,1} = \mu_{S,2} \quad (14)$$

$$\mu_{I,1} = \mu_{I,2} \quad (15)$$

$$\mu_{M,1} = \mu_{M,2} \quad (16)$$

Thus, by complementing the six equations Eqs. 11–16 with suitable correlations for the chemical potentials and the specific volumes of the two phases as a function of state variables, the equilibrium concentrations of the low molecular weight species can be determined at each time point by solving the corresponding set of nonlinear algebraic equations by standard numerical methods.

Different approaches are available for evaluating the thermodynamic properties of the different phases. Cubic equations of state such as the Peng–Robinson equations [58–60] can be used, or more comprehensive approaches suitable for polymeric systems, such as the statistical associating fluid theory [61, 62], the perturbed hard-sphere chain model [63], the Simha–Somcynski lattice-hole theory [64, 65], and the lattice theory of Sanchez and Lacombe [66]. Moreover, when dealing with compressible systems (gaseous continuous phase), the system pressure is also unknown and can be evaluated by imposing the following additional constraint:

$$V_R = V_1 + V_2 \quad (17)$$

where V_R is the reactor volume. In this context, the Sanchez–Lacombe equation of state is widely used for its ability to correlate pressure, volume, and temperature (PVT) data [23, 42, 43] and the equilibrium of multicomponent polymeric systems [67].

On the other hand, although equations of state provide both the volumes of the two phases and the chemical potentials of the species in a single theoretical framework, they are quite demanding in terms of computational effort. When such a detailed thermodynamic description is not required, the complexity of the mathematical treatment can be reduced by using simplistic equations such as the

volume additivity rule and expressing the equilibrium conditions using oversimplified, constant partition coefficients [47]. Accordingly, Eqs. 14–16 simplify to:

$$\frac{[S_1]}{[S_2]} = K_S \quad (18)$$

$$\frac{[I_1]}{[I_2]} = K_I \quad (19)$$

$$\frac{[M_1]}{[M_2]} = K_M \quad (20)$$

Whatever the selected approach, accurate prediction of the interphase partitioning at equilibrium is a prerequisite for any reliable model of polymerization in heterogeneous systems. Therefore, the parameters of the chosen thermodynamic model should always be determined from independent equilibrium data [47, 67, 68].

For high molecular weight species (active chains), the corresponding partition coefficients α_n are also needed to evaluate the driving force in the interphase transport in terms of Eqs. 7 and 8. Such evaluation is less established than in the case of low molecular weight species and is discussed separately in Sect. 3.4.

3.3 Kinetic Rate Constants

As is always the case in polymerization modeling, reliable evaluation of kinetic parameters is a difficult task, but crucial for ensuring that the model has good predictive ability. This is even more problematic in heterogeneous systems such as found in precipitation and dispersion polymerizations, where the values of such rate constants are needed for both phases.

For the continuous phase, the rate constants of initiator decomposition, propagation, and termination are generally expressed using Arrhenius-type expressions that account for the temperature and pressure effect:

$$k(T, p) = A \exp\left(-\frac{E + \Delta V^\#(p - p_{\text{ref}})}{RT}\right) \quad (21)$$

where A is a constant pre-exponential factor, E the thermal activation energy, $\Delta V^\#$ the activation volume, and p_{ref} a reference pressure. The rate constants calculated according to Eq. 21 are the intrinsic rate constants that reflect the chemistry of the system. Because the continuous phase is often characterized by low viscosity, in most cases these values apply throughout the polymerization reaction so that chain-length and conversion dependencies can be neglected.

For the dispersed phase, at the high polymer loadings typical of the particles (>50% by weight) the rate parameters become diffusion controlled, with values several orders of magnitude smaller than found in polymer-free systems [69–71]. Among the many approaches reported in the literature for the evaluation of diffusion-controlled kinetic constants [71, 72], a very convenient approach was developed in the frame of the collision theory of chemical reactions in liquids [73] together with a Fickian description of the diffusion process. Accordingly, considering two reacting species A and B, the effective rate constant, k_{eff} , can be estimated as [71, 74]:

$$\frac{1}{k_{\text{eff}}} = \frac{1}{k} + \frac{1}{4\pi r_{\text{AB}} D_{\text{AB}} N_{\text{A}}} \quad (22)$$

where k is the intrinsic rate constant, r_{AB} is the radius of collision of the two considered reacting species (i.e., the distance at which A and B react instantaneously), and D_{AB} is the mutual diffusion coefficient.

For propagation, a reasonable estimate of the radius of collision is given by the monomer molecular diameter σ . The mutual diffusion coefficient between radical and monomer is assumed equal to the sum of the respective self-diffusion coefficients. Under diffusion-controlled regimes, the monomer diffuses much faster than long radicals (i.e., $D_{\text{M}} \gg D_{\text{R}}$), therefore it follows that:

$$D_{\text{AB}} = D_{\text{MR}} = D_{\text{M}} + D_{\text{R}} \cong D_{\text{M}} \quad (23)$$

and the propagation rate constant in the dispersed phase can be expressed as:

$$\frac{1}{k_{p,2}} = \frac{1}{k_{p,1}} + \frac{1}{4\pi\sigma D_{\text{M},2} N_{\text{A}}} \quad (24)$$

where the intrinsic rate constant of propagation has been set equal to the value in the continuous phase, $k_{p,1}$.

For the termination reaction between two radicals of length n and m , the mutual diffusion coefficient is the sum of different contributions, that is, the center of mass diffusion coefficients of the two radicals, D_n and D_m , and the diffusion due to chain growth (the so-called propagation diffusion). Accordingly, the rate constant for the termination reaction in the dispersed phase, $k_{t,nm,2}$, is given by [43, 48]:

$$\frac{1}{k_{t,nm,2}} = \frac{1}{k_{t,1}} + \frac{1}{4\pi r_{nm} N_{\text{A}} (D_{n,2} + D_{m,2} + \frac{a^2}{3} k_{p,2} [M]_2)} \quad (25)$$

where the intrinsic rate constant of termination is again set equal to the value in the continuous phase, $k_{t,1}$ and a is the root-mean end-to-end distance divided by the square root of the number of monomer units in the chain. In their analysis of diffusion-controlled termination, Russell et al. [69] estimated the parameters

a and σ for three different polymerization systems, finding in all cases that their numerical values were quite similar. Accordingly, one can conveniently approximate a as equal to the monomer diameter σ [48]. The radius of collision for the radicals, r_{nm} , ranges from the lower bound $r_{nm} = \sigma$ to the upper bound $r_{nm} = 2aj_c^{1/2}$, with $j_c^{1/2}$ being the entanglement spacing [69, 71].

For the initiation reaction, the corresponding rate constant is frequently set to the same value for both phases (i.e., $k_{d,1} = k_{d,2}$). This assumption is substantiated by the observation that the medium composition has a major impact on efficiency and much less impact on the dissociation rate constant itself [70]. Accordingly, all diffusion limitation effects on the initiation step, relevant for the polymer-rich phase, can be accounted for in terms of reduced efficiency, which is expressed as a function of the diffusion coefficient of the initiator, D_1 , as:

$$f_2 = \left[1 - \frac{D_{1,0}}{D_1} \left(1 - \frac{1}{f_{2,0}} \right) \right]^{-1} \quad (26)$$

where $D_{1,0}$ and $f_{2,0}$ represent the diffusion coefficient and efficiency in the polymer-free system, respectively, with the latter value being equal to that for the continuous phase ($f_{2,0} = f_1$).

3.4 Transport Parameters

As anticipated, the rate of radical interphase transport can be expressed as the product of the overall transport coefficient, the particle surface area, and a driving force (difference in radical concentrations). Given the impact of this transport rate on the model results, its evaluation deserves special attention.

The simplest approach is to neglect all dependencies of the two parameters K_n and A_p (mainly upon chain length and particle size) while using their product $K_n A_p$ as a single, constant parameter to be evaluated by direct fitting to the experimental data. Focusing on the cases of major practical interest (small α values), this approach is particularly convenient when full separability between particle morphology and polymerization kinetics can be assumed and an accurate value of this parameter is not strictly required. This is the case for systems exhibiting limiting segregated behavior ($K_n A_p \ll 1$; quadrant I in Fig. 2) or when the dispersed phase is the dominant reaction locus ($K_n A_p \gg 1$; quadrant IV in Fig. 2). On the other hand, for all intermediate cases, a more detailed evaluation is required. Let us therefore consider the evaluation of K_n and A_p separately.

The overall mass transport coefficient of radicals between the continuous and dispersed phases is conveniently evaluated using the two-film theory as [57]:

$$\frac{1}{K_n} = \frac{\delta}{D_{n,1}} + \frac{\delta\alpha_n}{D_{n,2}} \quad (27)$$

where δ is the thickness of the diffusive boundary layer, which can be approximated as the particle radius; $D_{n,j}$ is the diffusion coefficient of the radicals of length n in phase j ; and α_n is the equilibrium partition coefficient as given by Eq. 3 for the radicals of length n . The diffusion coefficient of a radical of length n can be expressed as a function of the diffusion coefficient of the monomer, D_M , through the empirical correlation proposed by Griffiths et al. [75], where the scaling coefficient of the diffusion coefficient with the number of repeating units is an explicit function of the polymer weight fraction ω_P :

$$D_n = D_M n^{-(0.664+2.02\omega_P)} \quad (28)$$

Several models can be applied to evaluate the diffusion coefficient of the monomer, D_M , in a polymer rich-phase [76]. Those based on the free-volume concept, and especially those based on the formulation of Vrentas and Duda [77], are some of the more powerful for application in polymer reactions [38, 41, 42, 70, 71]. According to Vrentas and Duda [77], the diffusion coefficient of the monomer is given by:

$$D_M = D_{M,0} \exp\left(-\frac{E}{RT}\right) \exp\left(-\frac{\gamma(\omega_M V_M^* + \xi_{MS}\omega_S V_S^* + \xi_{MP}\omega_P V_P^*)}{V_{FH}}\right) \quad (29)$$

where $D_{M,0}$ is a constant, pre-exponential coefficient, E is the activation energy for the jump process of the diffusing molecule, γ is the overlap factor, V_i^* is the critical hole free volume required for molecule i to “jump” into, ξ_{Mj} is the ratio between the molar volumes of monomer and molecule j , and V_{FH} is the total system free volume. Despite the large success of this formulation, its main drawback is that a large number of parameters are involved whose determination is not always trivial. To overcome this issue, Zielinski and Duda [78] and Vrentas and Vrentas [79] proposed general procedures and guidelines for independent determination of most of the required parameters. More recently, Costa and Storti [80] proposed an alternative formulation of the free-volume theory in which the self-diffusion coefficient of the monomer is expressed as:

$$D_M = D_{M,0} \exp\left(-\gamma \frac{(\omega_M/\rho_M^* + \xi_{MS}\omega_S/\rho_S^* + \xi_{MP}\omega_P/\rho_P^*)}{1/\rho - 1/\rho_{\text{mix}}}\right) \quad (30)$$

where ρ_i^* and ρ_{mix}^* are the close-packed density of species i and of the mixture, respectively, and ρ is the density of the system. The main advantage of Eq. 30 over Eq. 29 is the use of the Sanchez–Lacombe lattice theory to estimate most of the required parameters, thus simplifying the parameter evaluation problem associated with the evaluation of D_M .

The partition coefficient for the radicals, α_n , can be expressed as a function of the chain length n through semi-empirical correlations, such as that proposed by Kumar et al. [81]:

$$\log \alpha_n = \log \alpha_x + \beta(n - n_x) \quad (31)$$

where the scaling coefficient β and the parameters α_x and n_x are determined by fitting experimental data [81, 82].

Finally, let us consider the evaluation of the parameter A_p , the link between particle morphology and polymerization kinetics. Having assumed a constant number of particles, N_p , one can estimate its value through the following equation:

$$N_p = \frac{3m_f}{4\pi\rho r_f^3} \quad (32)$$

where m_f is the mass of polymer of density ρ in the reactor at the end of the reaction and r_f is the final radius of the particles. Once the number of particles is known, the overall interphase area at the generic reaction time is easily evaluated as:

$$A_p = N_p 4\pi r_p^2 \quad (33)$$

where the actual radius of the particles, r_p , is given by:

$$r_p = \left(\frac{3 V_2}{4\pi N_p} \right)^{1/3} \quad (34)$$

Note that Eqs. 32–34 imply the assumption of monodisperse spherical particles. Although quite crude, this assumption was accurate enough to predict the effect of A_p on the system kinetics in several instances, as shown in the next section. Additionally, it has the advantage of providing a simple way of estimating A_p through accessible experimental quantities such as the polymer mass at the reaction end and the final particle radius. Finally, for systems leading to fully amorphous morphologies where no average particle radius can be easily defined (typically precipitation polymerizations), one can still use Eqs. 33 and 34 to account for the change in overall area during the reaction by treating N_p as a fitting parameter [44, 46].

4 Applications

Three case studies are presented to illustrate the general reliability of the modeling approach for widely different systems: the precipitation copolymerization of vinyl-imidazole (VI) and vinyl-pyrrolidone (VP) in an organic solvent, the precipitation/dispersion copolymerization of vinylidene fluoride (VDF) and hexafluoropropylene (HFP) in scCO_2 , and the precipitation polymerization of vinyl chloride carried out in suspension.

4.1 Precipitation Polymerization in Organic Solvent

The precipitation copolymerization of VI and VP in butylacetate was investigated experimentally by Arosio et al. [83]. Let us first briefly summarize the experimental evidence concerning the impact of particle morphology on the polymerization kinetics, which is the key to identification of the relative contribution of the two phases to the polymerization and their possible interplay in the overall kinetics. A representative SEM image of the copolymer collected at the end of the reaction is shown in Fig. 3. Although the primary particles do not coalesce completely and keep their identity during the whole reaction, they aggregate in large clusters.

Analysis of the impact of mixing rate on the size distribution of clusters has shown that the combination of aggregation and breakage induced by shear leads to

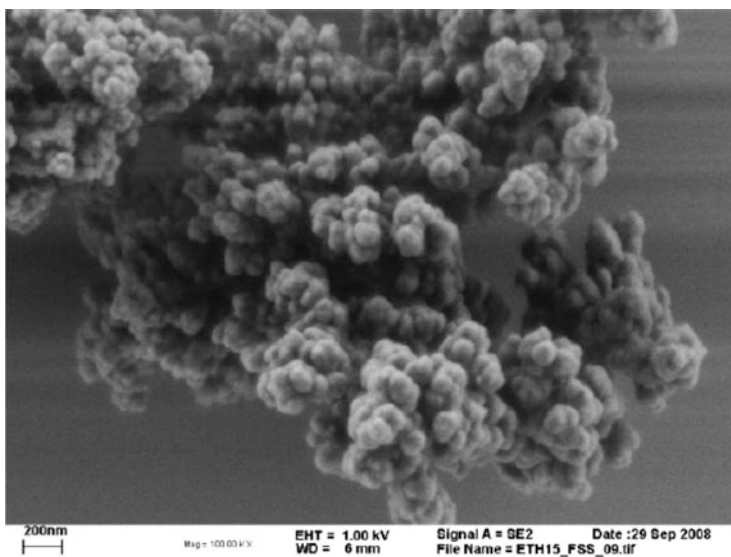


Fig. 3 SEM picture of polymer aggregates obtained at the end of VI/VP precipitation reactions. (Reprinted with permission from Arosio et al. [83]. Copyright 2011 Wiley)

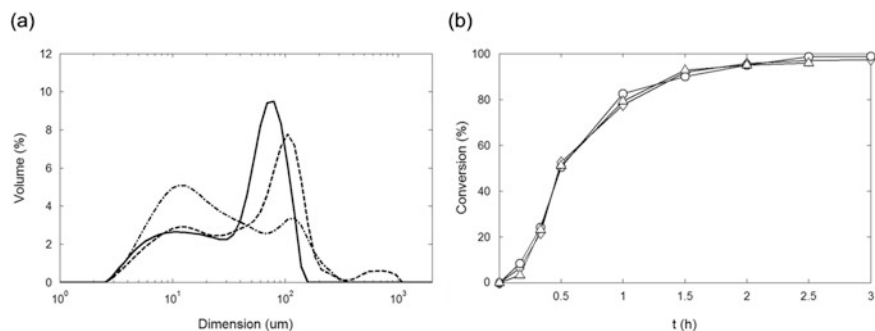


Fig. 4 Precipitation copolymerization of VI/VP (75/25 w/w). (a) Effect of stirring rate on the final particle size distribution: 100 (dash-dotted line), 200 (dashed line), and 300 rpm (continuous line). (b) Effect of stirring rate on monomer conversion: 100 (triangle), 200 (circle), and 300 rpm (diamond). (Adapted with permission from [83]. Copyright 2011 Wiley)

polydisperse aggregates covering a wide range of sizes (1–1,000 μm), with particle size distribution heavily affected by the mixing rate (Fig. 4a). In contrast, the reaction rate is not affected by the shear rate (Fig. 4b). Because the overall interphase area is a function of the average size of the particles and does not seem to affect the kinetics, the experimental evidence implies that the rate of radical interphase transport does not play a relevant role in the polymerization kinetics. More explicitly, evolution of the polymerization reaction and evolution of particle size can be fully separated and viewed as two independent processes.

In terms of Ω parameters, for $\Omega_2 \ll 1$, because the copolymer is fully insoluble in the continuous phase, the “separation” mentioned above corresponds to two possible limiting cases: (1) negligible transport of the radicals, leading to a segregated system ($\Omega_1 \ll 1$), or (2) very fast and irreversible transport of the radicals from the continuous to the dispersed phase ($\Omega_1 \gg 1$). From the model perspective, these two options correspond to setting negligible or extremely high values for the product KA_p , respectively, in both cases safely neglecting all functional dependencies of the same parameters. Accordingly, the rate of transport can be modeled assuming negligible solubility of radical oligomers in the solvent-rich phase ($\alpha = 0$) and a single lumped parameter, the product KA_p [47].

Using an additional series of simplifying assumptions (monomer partitioning in terms of constant partition coefficients; conversion-independent values of the rate parameters for the reactions of initiation, propagation, and termination; diffusion limitations on the termination rate constant simplistically accounted for by using a parameter value for the polymer-rich phase two orders of magnitude smaller than that for the solvent-rich phase), the number of fitting parameters can be reduced to three: the lumped transport parameter, KA_p ; the partition coefficient of the initiator, K_i ; and the rate constant of the crosslinking reactions taking place in the dispersed phase (these reactions need to be considered because of the presence of VI in the polymer backbone [84, 85]).

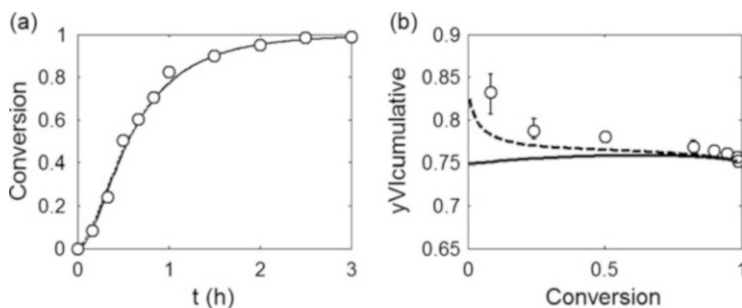


Fig. 5 Comparison between model and experimental data: (a) conversion versus time and (b) copolymer composition in terms of cumulative VI fraction. Model simulations correspond to initiator preferentially partitioned in the polymer phase, $K_I = 0.01$, and negligible transport leading to a segregated system (*dashed line*), or to $K_I = 0.01$ and extremely fast transport with the reaction occurring predominantly in the polymer phase (*continuous line*). Experimental data (*circle*) for VI/VP = 75/25. (Adapted with permission from Arosio et al. [47]. Copyright 2011 Wiley)

The last parameter only affects the polymer molecular weight, therefore a set of parametric simulations were initially carried out neglecting this specific reaction at different values of KA_p and K_I to elucidate the contribution of each reaction locus and the specific operative situation (segregation with two loci or irreversible transport with a dominant locus). Four limiting cases were considered: complete segregation ($KA_p = 0$), with preferential initiator partitioning in the continuous ($K_I = 100$) or dispersed phase ($K_I = 0.01$), and extremely fast transport ($KA_p \gg 0$) again with the same two extreme values of K_I . The model results clearly indicated that initiator partitioning in the dispersed phase is dominant. The effect of transport rate is shown in terms of conversion versus time in Fig. 5a and of copolymer composition versus conversion in Fig. 5b. Even though the reaction rate is practically identical whatever the KA_p value, it is interesting that the copolymer composition is quite different and closer to the experimental case when radical segregation is operative. This is because the compositions of the chains formed in the two phases are quite different: VI-richer chains are formed in the continuous phase rather than in the dispersed phase and, during the reaction, the increasing relevance of the particle phase is reflected by the corresponding change in copolymer composition. Although such a transition is almost complete at around 20% conversion, the copolymer is produced in both phases throughout the reaction, with a final contribution of the continuous phase of about 10%.

The model results in terms of MWD are compared with experimental data in Fig. 6, which also shows the contribution of the polymer produced in each phase as predicted by the model. The general agreement is quite good. Both overall distributions exhibit a clear shoulder in the high molecular weight region as a result of the crosslinking reactions mentioned above. Most of the chains are produced in the dispersed phase and all crosslinked chains are part of this population (i.e., they are

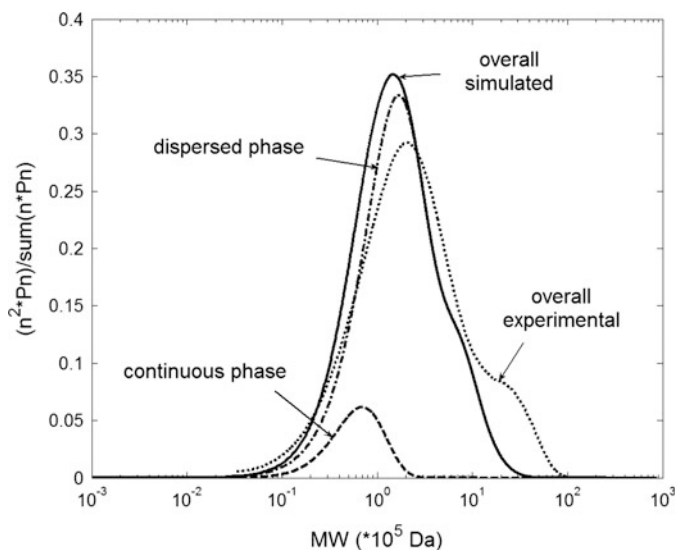


Fig. 6 Precipitation copolymerization of VI/VP (75/25 w/w). Final molecular weight distributions: experimental (*dotted line*), overall simulated (*continuous line*), contribution of the continuous phase (*dashed line*), and contribution of the dispersed phase (*dash-dotted line*). (Reprinted with permission from Arosio et al. [47]. Copyright 2011 Wiley)

formed in the particles). The continuous phase contributes to the overall MWD with only a small fraction of chains in the low molecular weight region, thus resulting in further broadening of the overall distribution. Most of these chains are produced in the early phases of the reaction, when the amount of polymer-rich phase is negligible. As the reaction proceeds, and the volume of the polymer particles increases, the initiator is mainly present within the polymer aggregates ($K_I = 0.01$) and the dominant reaction locus shifts from the continuous to the dispersed phase, which, eventually, contributes the most to polymer formation.

Finally, model and estimated parameter values were conclusively validated by the set of predictive simulations of conversion versus time compared with the experimental results (see Fig. 7). The impacts of monomer composition (Fig. 7a) and initiator concentration (Fig. 7b) are well captured by the model.

To conclude, the developed model – although very simplified – provides a reliable description of the reaction kinetics and enables sound interpretation of the experimental results. Additionally, a preliminary analysis in terms of Ω parameters, supported by some experimental evidence, provides effective conceptual understanding of the main process features, thus enabling identification of reasonable assumptions to be applied in model development without significantly affecting the predictive capabilities of the model.

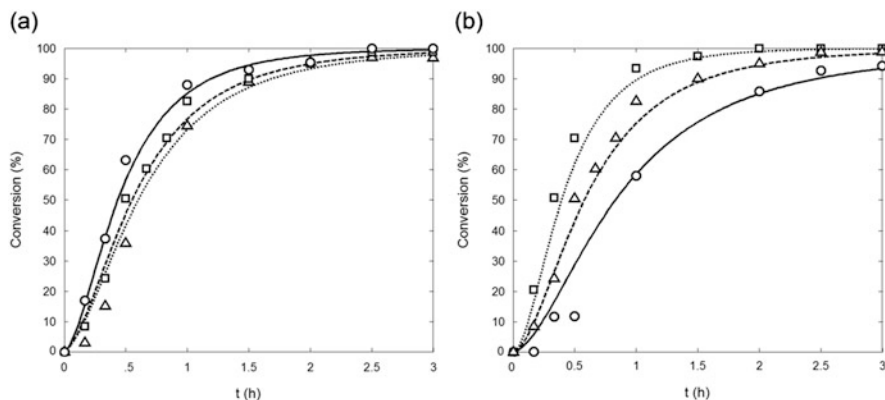


Fig. 7 Precipitation copolymerization of VI/VP. (a) Effect of monomer composition on conversion for VI/VP (w/w) ratios of 90:10 (*triangle*), 75:25 (*square*), and 50:50 (*circle*). (b) Effect of percentage initiator concentration on conversion (VI/VP w/w = 75:25) for 0.3 (*circle*), 0.6 (*triangle*), and 1.2% (*square*) initiator. (Adapted with permission from Arosio et al. [47]. Copyright 2011 Wiley)

4.2 Precipitation and Dispersion Copolymerizations in Supercritical Carbon Dioxide

We now focus on a different system, specifically on the binary system VDF-HFP polymerized in sCO_2 , a fluorinated material of industrial relevance usually produced in emulsion [86]. The impact of the interphase area on the copolymer MWD was investigated by comparing experiments carried out at different amounts of a perfluoropolyether surfactant [24], which was found especially effective for producing narrowly distributed spherical particles in VDF homopolymerization [23, 87]. SEM pictures of the copolymer particles produced in batch at an initial monomer mole fraction $f_{\text{HFP}} = 0.2$ without and with stabilizer (precipitation and dispersion) are shown in Fig. 8. The images reveal that microparticles are clearly formed in both cases. Given the plasticizing effect of the supercritical medium, coalesced particles do not retain their identity. Without stabilizer (Fig. 8a), the extent of coalescence is significant, resulting in a copolymer matrix composed of irregularly shaped particles with broad size distribution. With stabilizer (Fig. 8b), the particles are still partly coalesced but more spherical and, most importantly, better segregated, with an average diameter two to three times smaller than in the precipitation case. Accordingly, a value of A_p two to three times larger (the particle number is larger in the dispersion case) under otherwise identical conditions was estimated in the dispersion case.

Although the difference in interphase areas is small, a striking difference between the two processes is found when looking at the corresponding MWDs (see Fig. 9). A bimodal distribution is obtained by precipitation polymerization, with clearly distinct lower and higher molecular weight modes, whereas a broad but monomodal distribution is found under dispersion conditions. These experimental results indicate a major impact of radical transport (i.e., of interphase area A_p) on

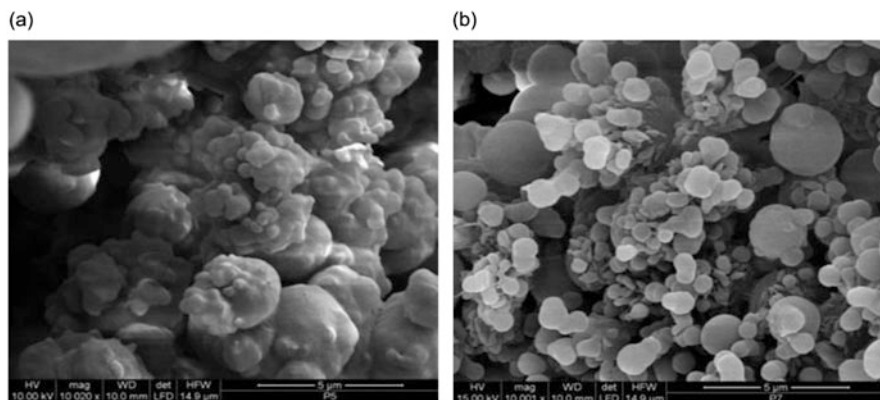


Fig. 8 SEM pictures of VDF-HFP copolymer produced in scCO_2 by (a) precipitation and (b) dispersion. (Adapted with permission from Costa et al. [24]. Copyright 2010 American Chemical Society)

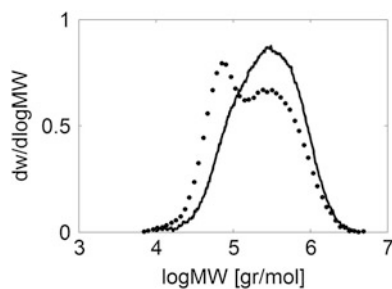


Fig. 9 Experimental molecular weight distributions of VDF-HFP copolymers produced by precipitation (*symbols*) and dispersion (*continuous line*); $T = 50^\circ\text{C}$, $t = 6$ h, $[M] = 5.5$ mol L^{-1} , $f_{\text{HFP}} = 0.2$. (Reprinted with permission from Costa et al. [24]. Copyright 2010 American Chemical Society)

the reaction kinetics. Again, given the negligible value of Ω_2 , parameter Ω_1 regulates the process and its value is expected to be close to 1, so that a small increase in the interphase area can horizontally shift the position of the operating point in Fig. 2 from the first to fourth quadrant, that is, from segregated (two loci) to dominant reaction in the polymer-rich phase (one locus). As a consequence, the system requires a more detailed description of radical interphase transport than in the VI/VP case. Accordingly, diffusion limitations and chain-length dependencies were taken into account for all the rate parameters, as well as for the overall transport coefficient, by using the correlations previously described in Sect. 3 (cf. [48]). With respect to the partitioning of low molecular weight species, the Sanchez–Lacombe equation of state was used for the monomers and for CO_2 , whereas equipartitioning (in mass) was assumed for the initiator.

The predictions of a model of this type in terms of time evolution of the MWD are compared with experimental results in Fig. 10a, c for precipitation and in

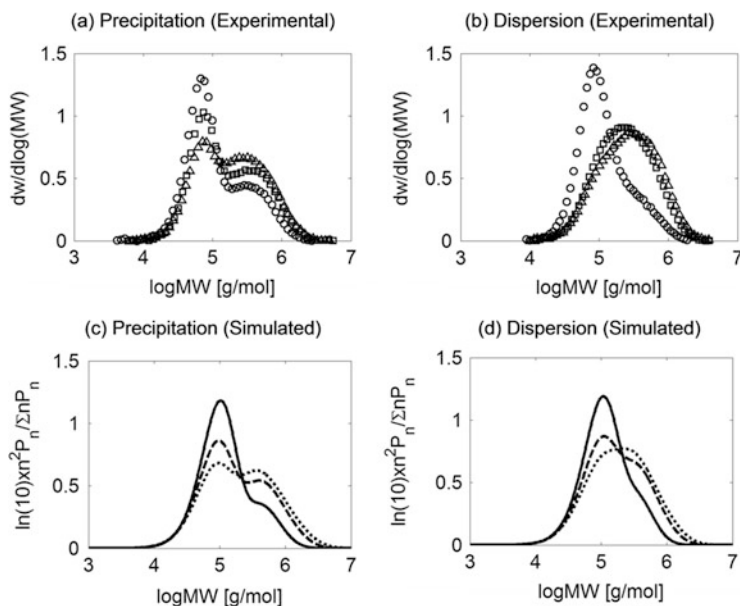


Fig. 10 Time evolution of molecular weight distribution of VDF-HFP copolymerization in scCO_2 for precipitation (*left*) and dispersion (*right*). *Top*: Experimental data after a reaction time of 60 (*circle*), 180 (*square*), and 360 min (*triangle*). *Bottom*: Calculated MWD after 60 (*continuous line*), 180 (*dashed line*), and 360 min (*dotted line*). (Adapted with permission from Costa et al. [48]. Copyright 2012 Wiley)

Fig. 10b, d for dispersion. In all cases, the agreement between model and experiments is quite remarkable, thus enabling a sound mechanistic interpretation of the results. The two MWD modes formed during the precipitation reactions are representative of copolymer chains produced in the continuous phase (lower MW mode) and in the dispersed phase (higher MW mode), respectively. The lower MW mode initially prevails, indicating that in the early phases of the reaction the continuous phase is the dominant reaction locus, which is always the case in unseeded batch reactions. However, as the reaction proceeds, the interphase area increases because of the increasing amount of polymer, and, in turn, the dispersed phase progressively becomes the dominant reaction locus. As a result, the relative contribution of the higher molecular weight mode to the overall MWD increases with time, as is clearly shown in Fig. 10 by both the experimental data and the model results. For dispersion reactions, a similar transition of the dominant reaction locus is observed. Nevertheless, because the particles are smaller than in the precipitation case, the resulting A_p is larger and the rate at which the radicals generated in the continuous phase are transported to the particles is enhanced, which makes the transition of the dominant locus of reaction occur more quickly. Eventually, most of the chains are terminated in the dispersed phase, and a broader but monomodal distribution is obtained.

Changing the monomer composition has a similar effect on the final MWD, as shown in Fig. 11 for dispersion copolymerization. A high molecular weight,

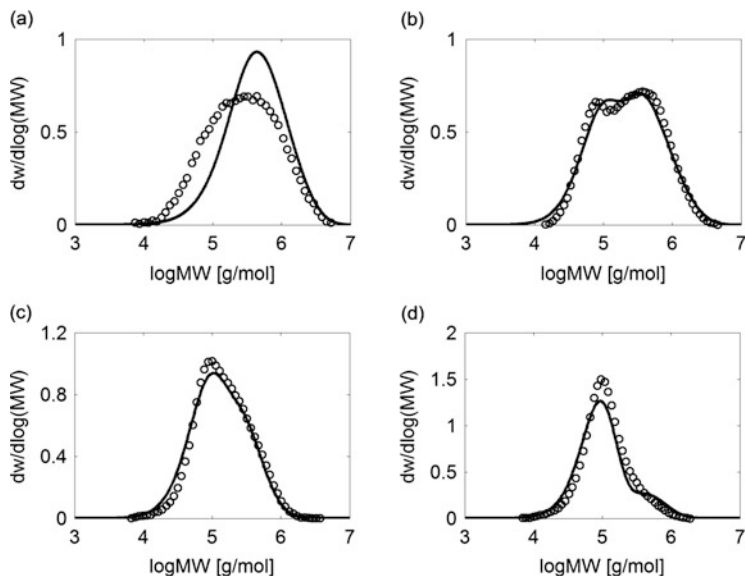


Fig. 11 Experimental (*circle*) and calculated (*line*) molecular weight distributions for VDF-HFP dispersion copolymerization; $T = 50^{\circ}\text{C}$, $t = 3\text{ h}$, $[\text{M}] = 5.5\text{ mol L}^{-1}$. Initial monomer mole fraction f_{HFP} is (a) 0, (b) 0.15, (c) 0.3, and (d) 0.4. (Adapted with permission from Costa et al. [48]. Copyright 2012 Wiley)

monomodal distribution is obtained when VDF alone is fed to the reactor (Fig. 11a). As the amount of HFP in the recipe increases, the distribution gradually shifts toward lower molecular weights: the MWD is clearly bimodal at intermediate HFP content (Fig. 11b), and the lower molecular weight peak becomes dominant at higher HFP content (Fig. 11c, d). The model captures all distributions and their transition remarkably well. From the model perspective, several factors contribute to the shift in distribution toward the lower MW mode as f_{HFP} increases [48]. First, HFP is significantly less reactive than VDF. Therefore, for the same reaction time, the amount of produced copolymer, and therefore the interphase area A_p , decreases with increasing HFP content. Additionally, the richer the system is in HFP, the lower the transport parameters of the growing radicals and the lower the monomer concentration in the polymer particles, which is a result of the composition-dependent partitioning of these monomers. Furthermore, the effectiveness of the surfactant deteriorates progressively as the content of HFP in the system increases [24], resulting in a reduction in the overall number of particles and, again, in the specific interphase area. Thus, VDF homopolymer dispersions are characterized by faster radical transport rates (larger Ω_1 values) and higher reactivity in the polymer-rich phase. This is the main reaction locus and a monomodal high MWD is obtained (Fig. 11a). In contrast, dispersion reactions carried out at high HFP concentrations (Fig. 11d) are characterized by slower radical transport rates and low reactivity in the polymer phase. Under these conditions, the continuous phase (where shorter

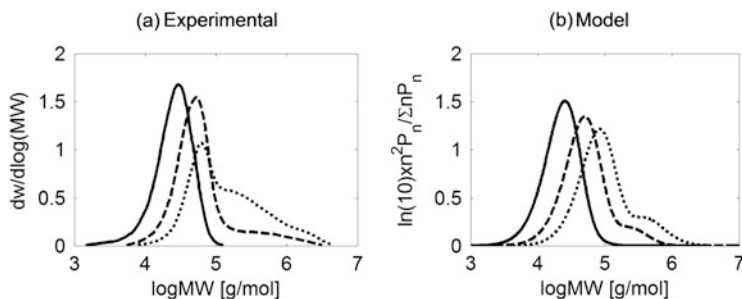


Fig. 12 Effect of total monomer concentration on molecular weight distribution produced in a continuous stirred tank reactor under precipitation conditions. Experimental data from Ahmed et al. 2007 (left) and model predictions (right). Operative conditions: $T = 40^{\circ}\text{C}$, $f_{\text{HFP}} = 0.265$, residence time $\tau = 20$ min. Monomer feed concentrations are 1.96 (solid curves), 3.92 (dashed curves), and 6.53 mol L^{-1} (dotted curves). (Adapted with permission from Costa et al. [48]. Copyright 2012 Wiley)

chains are produced) prevails as reaction locus, whereas the small fraction of chains terminating inside the particles results in MWD tailing at high molecular weights.

The predictive capabilities of the same kinetic model were further verified using independent data obtained in a continuous stirred tank reactor [88]. The effect of increasing monomer concentration for precipitation copolymerization at $f_{\text{HFP}} = 0.27$ is shown in Fig. 12, together with the corresponding model predictions. At low monomer concentration, the small amount of polymer particles present in the system captures a negligible amount of radicals, and the continuous phase is practically the only reaction locus. The distribution is therefore narrow and monomodal. As total monomer content increases, more radicals are captured because of the larger interphase area of the polymer particles and the contribution of the particle phase to the kinetics progressively increases, leading to the formation of high molecular weight tails. Although the comparison between model results and experimental data is not as good as in the previous examples, the model still captures the relevant features of the distributions and allows straightforward interpretation of the appearance of the high molecular weight tailing at increasing monomer concentration. This result appears especially significant when considering that, in this case, the model was used in a fully predictive way.

4.3 Precipitation Polymerization of Vinyl Chloride

Poly(vinyl chloride) (PVC) is a commodity polymers with one of the largest production capacities and is mostly produced by suspension polymerization [41, 89]. In suspension polymerization, the monomer is initially dispersed in water as 50–500 μm droplets by the combined effects of mechanical agitation and surfactant stabilization. Monomer-soluble initiators are used, so the entire

polymerization reaction takes place inside these droplets and each droplet can be considered a small, bulk polymerization reactor. However, PVC is insoluble in its monomer and precipitates as soon as it is formed. Therefore, a precipitation polymerization regime is established within each monomer droplet. The droplet is finally converted into a PVC grain composed of a porous network of packed polymer particles [89, 90]. In view of the industrial relevance of this process, the mechanism of formation and evolution of the internal morphology of the grain with the reaction progress has been studied extensively, both experimentally and through modeling [90–94]. After a short nucleation phase, completed within the first few percent of monomer conversion, primary polymer particles of 0.2–1.5 μm are formed. The particles then grow by polymerization of the absorbed monomer and by further precipitation of polymer formed in the monomer phase. Additionally, the particles aggregate and coalesce as the reaction proceeds. The interplay between growth, aggregation, and coalescence finally determines the internal morphology and porosity of the grains. The extent of aggregation and coalescence of the primary particles in this system is influenced by many parameters (temperature, mixing, nature of the suspending medium, nature and concentration of stabilizers, etc.), meaning that the estimation of the interphase area between the polymer and the monomer phases is a challenging task. On the other hand, it has been observed that aggregation is significant even at low conversions, giving rise to a densely packed morphology similar to that observed for VI/VP precipitation (see Fig. 3 with SEM images reported by Smallwood for PVC [90]). Accordingly, as for the VI/VP case, one can expect that the total effective amount of interphase area available for radical interphase transport is also quite small in this system. The assumption of a segregated system (regime I in Fig. 2) for PVC precipitation polymerization thus appears reasonable and has often been applied. As representative examples, Crosato-Arnaldi et al. [34], Abdel-Alim et al. [37], and Kiparissides et al. [41] successfully applied two-phases models without interphase transport (segregated models) to describe the kinetics of PVC suspension polymerization.

More recently, the validity of the assumption of a fully segregated system was evaluated by Wieme et al. [45], who also included a term for radical interphase transport in the two-phase model. The authors used the two-film theory for the overall mass transfer coefficient (Eq. 27), and, to take into account the decrease in particle concentration as a result of coalescence, they did not assume constant particle concentration and assumed the following empirical relationship:

$$n_p = n_p^0 \exp(-\gamma X) \quad (35)$$

where $n_p = N_p/(V_1 + V_2)$, and the two adjustable parameters n_p^0 and γ represent the initial volumetric concentration of polymer particles and the decay parameter, respectively. Thus, the evolution of the overall interphase area and the rate of radical interphase transport throughout the reaction can be calculated using Eqs. 33–35. In particular, in agreement with experimental observations [90], n_p^0 increases with decreasing temperature, implying that A_p , and thus the flow of radicals precipitating

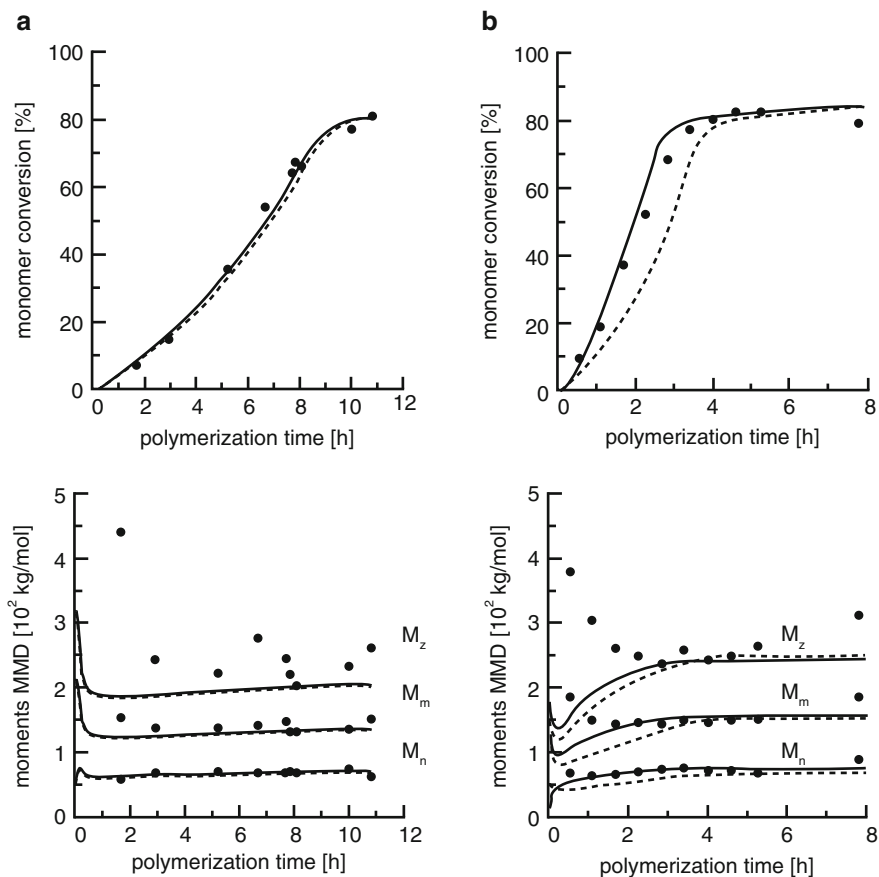


Fig. 13 Effect of temperature on conversion (*top*) and average molecular weights (*bottom*) for PVC suspension polymerization at (a) $T = 318$ K with 0.02354 wt% of *tert*-butyl peroxyneodecanoate initiator, (b) $T = 308$ K with 3.02 wt% of *tert*-butyl peroxyneodecanoate initiator. Model simulations are shown as *dashed lines* for the segregated, two-loci model (without radical transfer) and as *continuous lines* for the complete two-loci model (with radical transfer). (Adapted with permission from Wieme et al. [45]. Copyright 2009 Wiley)

from phase 1 to phase 2, increases with decreasing temperature. Note that this model reduces to the segregated case by setting $n_p = 0$ (i.e., no interphase area available for radical transport). Wieme et al. evaluated the unknown model parameters (including the intrinsic rate constants for propagation and termination in the monomer phase) for both cases (segregated and nonsegregated) by regression of conversion and average molecular weight data from experiments carried out at different temperatures [45]. Comparison of the predictions of both models with the experimental results is shown in Fig. 13 for the reactions at 318 K and 308 K. At the highest temperature (Fig. 13a), the two models provide almost identical results, indicating that the role of the radical interphase transport in this

case is negligible. The polymerization occurs independently in each phase but, as the reaction proceeds and the volume of the polymer phase increases at the expenses of the monomer phase, the main reaction locus shifts from the monomer to the polymer phase, resulting in an evident auto-acceleration effect. By contrast, at the lowest temperature (Fig. 13b), the difference between the two model results is appreciable, and the complete model performs better than the segregated one, especially in terms of conversion versus time. This finding can be attributed to the enhanced rate of radical interphase transport resulting from the increased number of particles at the lower reaction temperature. The steeper conversion profile obtained from the full model with respect to the segregated one indicates that the transfer of radicals, at least partly, accelerates the shift of the main reaction locus from the continuous to the dispersed phase. It is worth noting that, as shown in Fig. 13 (lower images), the two models do not differ significantly in terms of molecular weight evolution, the final average molecular weight being mainly dictated by chain transfer to monomer. Notably, this makes the discrimination of different models (with or without radical transfer) more difficult as they are based on conversion data only.

Thus, two loci models that account for the reaction occurring in both phases can provide a fairly accurate description of the system kinetics. Even though PVC suspension and precipitation polymerizations can be considered in most cases as fully segregated, given the high degree of aggregation and coalescence of the polymer particles, accounting for the interphase radical transport broadens the range of model applicability to experimental conditions that favor the formation of a larger interphase area.

5 Conclusions

The presence of more than one reaction locus, coupled with the complex interactions between particle morphology and polymerization kinetics, makes the kinetic modeling of dispersed polymerization systems particularly challenging. On the other hand, judicious selection of meaningful and reliable assumptions enables the separation of the mathematical descriptions of kinetics and particle size distribution in many cases, the overall interphase area being the only parameter connecting kinetics and particle morphology.

The impact of the interphase area on the polymerization kinetics can be rationalized in terms of dimensionless phase-specific quantities, the Ω parameters, defined as the ratios between the rate of radicals diffusing out of a phase and the rate of termination in the same phase. Based on the values of the Ω parameters for the two phases, different limiting regimes and the role of radical interphase transport can be readily identified. Because the solubility of high molecular weight species in the continuous phase is negligible in most cases of practical interest, the Ω parameter for the continuous phase is decisive. Its value determines the operating regime, ranging from complete radical segregation to complete transport of radicals

to the dispersed phase. Notably, the main reaction locus, and therefore the overall MWD, can be controlled by tuning the interphase area. Such tuning can be achieved by varying the hydrodynamics of the system (enhancing or reducing particle aggregation through shear) or its colloidal stability (reducing or increasing the amount of an effective stabilizer).

A modeling framework suitable for capturing all the main features mentioned above and representing a good compromise between the requirement for a detailed description and the need to keep the number of adjustable parameters to a minimum has been reviewed in this contribution. Moreover, some of the theoretical approaches and correlations commonly used in the field of polymer reaction engineering to estimate the model parameters have also been reported.

The proposed modeling approach has been validated through selected applications to homo- and copolymerizations in organic solvents and in supercritical media. Accurate predictions of the time evolution of conversion, copolymer composition, and MWD can be achieved with limited computational effort when a meaningful mechanistic picture is selected. In the examined case of precipitation copolymerization of VI and VP in organic solvent, the time evolution of the cumulative composition directly reflects the different copolymerization behaviors in the different phases. On the other hand, with reference to the production of VDF-based fluorinated copolymers in scCO_2 , control of the final MWD from monomodal to bimodal is obtained by tuning the stabilizer amount (i.e., by shifting the polymerization from dispersion to precipitation conditions). Each MWD mode represents the contribution of the polymer produced in a specific phase. In the case of precipitation polymerization of vinyl chloride, carried out either in bulk or in suspension, the high degree of aggregation and coalescence of the polymer particles allows segregated models to be applied in most cases. On the other hand, accounting for radical interphase transport expands the model applicability to all cases in which the experimental conditions favor the formation of a larger number of particles.

To conclude, the proposed approach represents a powerful tool for understanding the reaction mechanisms. In turn, the reliable quantitative description of process kinetics is a decisive tool for the design of optimal reaction paths and careful quality control of the final product. Although only free-radical polymerization has been considered, the general concepts and strategies presented here can be effectively applied to other polymerization mechanisms.

Acknowledgements The financial support of Swiss National Science Foundation (SNF Project 200021.153403/1) is gratefully acknowledged.

References

1. Barrett KEJ (1975) Dispersion polymerization in organic media. Wiley, London

2. Ober CK, Lok KP, Hair ML (1985) Monodispersed, micron-sized polystyrene particles by dispersion polymerization. *J Polym Sci Polym Lett Ed* 23:103–108
3. Tseng CM, YY Lu, El-Aasser MS, Vanderhoff JW (1986) Uniform polymer particles by dispersion polymerization in alcohol. *J Polym Sci A Polym Chem* 24:2995–3007
4. Richez AP, Yow HN, Biggs S, Cayre OJ (2013) Dispersion polymerization in non-polar solvent: evolution toward emerging applications. *Prog Polym Sci* 38:897–931
5. Almog Y, Reich S, Levy M (1982) Monodisperse polymeric spheres in the micron size range by a single step process. *Br Polym J* 14:131–136
6. IG Farbenindustrie AG (1933) GB Patent 434,783
7. Osmond DWJ, Thompson HH (1957) GB Patent 893,429
8. Osmond DWJ (1963) GB Patent 893,429
9. Rohm & Haas (1963) GB Patent 934,038
10. Barrett KEJ, Thomas HR (1969) Kinetics of dispersion polymerization of soluble monomers. I Methyl methacrylate. *J Polym Sci A-1* 7:2621–2650
11. Barrett KEJ (1973) Dispersion polymerization in organic media. *Br Polym J* 5:249–332
12. Cooper AI (2000) Polymer synthesis and processing using supercritical carbon dioxide. *J Mater Chem* 10:207–234
13. Byun HS, McHugh MA (2000) Impact of free monomer concentration on the phase behavior of supercritical carbon dioxide-polymer mixtures. *Ind Eng Chem Res* 39:4658–4662
14. Dinoia TP, Conway SE, Lim JS, McHugh MA (2000) Solubility of vinylidene fluoride polymers in supercritical CO₂ and halogenated solvents. *J Polym Sci B Polym Phys* 38:2832–2840
15. Hsiao YL, Maury EE, DeSimone JM (1995) Dispersion polymerization of methyl methacrylate stabilized with poly(1,1-dihydroperfluorooctyl acrylate) in supercritical carbon dioxide. *Macromolecules* 28:8159–8166
16. Romack TJ, Maury EE, DeSimone JM (1995) Precipitation polymerization of acrylic acid in supercritical carbon dioxide. *Macromolecules* 28:912–915
17. Berger T, McGhee B, Scherf U, Steffen W (2000) Polymerization of vinylpyrrolidone in supercritical carbon dioxide with a diblock copolymer stabilizer. *Macromolecules* 33:3505–3507
18. Carson T, Lizotte J, Desimone JM (2000) Dispersion polymerization of 1-vinyl-2-pyrrolidone in supercritical carbon dioxide. *Macromolecules* 33:1917–1920
19. Charpentier PA, DeSimone JM, Roberts GW (2000) Continuous precipitation polymerization of vinylidene fluoride in supercritical carbon dioxide: modeling the rate of polymerization. *Ind Eng Chem Res* 39:4588–4596
20. Galia A, Giaconia A, Iaia V, Filardo G (2004) Synthesis of hydrophilic polymers in supercritical carbon dioxide in the presence of a siloxane-based macromonomer surfactant: heterogeneous polymerization of 1-vinyl-2 pyrrolidone. *J Polym Chem A Polym Chem* 42:173–185
21. Tai H, Wang W, Howdle SM (2005) Dispersion polymerization of vinylidene fluoride in supercritical carbon dioxide using a fluorinated graft maleic anhydride copolymer stabilizer. *Macromolecules* 38:1542–1545
22. Beginn U, Najjar R, Ellmann J, Vinokur R, Martin R, Möller M (2006) Copolymerization of vinylidene difluoride with hexafluoropropene in supercritical carbon dioxide. *J Polym Chem A Polym Chem* 44:1299–1316
23. Mueller PA, Storti G, Morbidelli M, Costa I, Galia A, Scialdone S, Filardo G (2006) Dispersion polymerization of vinylidene fluoride in supercritical carbon dioxide. *Macromolecules* 39:6483–6488
24. Costa LI, Storti G, Morbidelli M, Ferro L, Scialdone O, Filardo G, Galia A (2010) Copolymerization of VDF and HFP in supercritical carbon dioxide: experimental analysis of the reaction loci. *Macromolecules* 43:9714–9723
25. Li GL, Möhwald H, Shchukin DG (2013) Precipitation polymerization for fabrication of complex core-shell hybrid particles and hollow structures. *Chem Soc Rev* 42:3628–3646
26. Pich A, Richtering W (2010) Microgels by precipitation polymerization: synthesis, characterization and functionalization. *Adv Polym Sci* 234:1–37

27. Zhang H (2013) Controlled/"living" radical precipitation polymerization: a versatile polymerization technique for advanced functional polymers. *Eur Polym J* 49:579–600
28. Sun JT, Hong CY, Pan CY (2013) Recent advances in RAFT dispersion polymerization for preparation of block copolymer aggregates. *Polym Chem* 4:873–881
29. Paine AJ, Luymes W, McNulty J (1990) Dispersion polymerization of styrene in polar solvents. 6. Influence of reaction parameters on particle size and molecular weight in poly (N-vinylpyrrolidone)-stabilized reactions. *Macromolecules* 23:3104–3109
30. Liu T, DeSimone JM, Roberts GW (2006) Kinetics of the precipitation polymerization of acrylic acid in supercritical carbon dioxide: the locus of polymerization. *Chem Eng Sci* 61:3129–3139
31. Costa LI, Storti G, Morbidelli M, Galia A, Filardo G (2011) The rate of polymerization in two loci reaction systems: VDF-HFP precipitation copolymerization in supercritical carbon dioxide. *Polym Eng Sci* 51:2093–2012
32. Jiang S, Sudol ED, Dimonie VL, El-Aasser MS (2008) Kinetics of dispersion polymerization: effect of medium composition. *J Polym Chem A Polym Chem* 46:3638–3647
33. Saenz JM, Asua JM (1998) Kinetics of the dispersion copolymerization of styrene and butyl acrylate. *Macromolecules* 31:5215–5222
34. Crosato-Arnaldi A, Gasparini P, Talamini G (1968) The bulk and suspension polymerization of vinyl chloride. *Makromol Chem* 117:140–152
35. Olay OF (1975) Ein einaches modell zur beschreibung der kinetic der vinylchlorid-polymerisation in substanz und in anderen fällungssystemen bei temperaturen um 50°C. *Angew Makromol Chem* 47:1–14
36. Avela A, Poersch HG, Reichert KH (1990) Modelling the kinetics of the precipitation polymerization of acrylic acid. *Angew Makromol Chem* 175:107–116
37. Abdel-Alim AH, Hamielec AE (1972) Bulk polymerization of vinyl chloride. *J Appl Polym Sci* 16:783–779
38. Saenz JM, Asua JM (1999) Mathematical modeling of dispersion copolymerization. *Colloids Surf A Physiochem Eng Asp* 153:61–74
39. Ahmed SF, Poehlein GW (1997) Kinetics of dispersion polymerization of styrene in ethanol. 1. Model development. *Ind Eng Chem Res* 36:2597–2604
40. Ahmed SF, Poehlein GW (1997) Kinetics of dispersion polymerization of styrene in ethanol. 2. Model validation. *Ind Eng Chem Res* 36:2605–2615
41. Kiparissides C, Daskalakis G, Achilias DS, Sidiropoulou E (1997) Dynamic simulation of industrial poly(vinyl chloride) batch suspension polymerization reactors. *Ind Eng Chem Res* 36:1253–1267
42. Chatzidoukas C, Pladis P, Kiparissides C (2003) Mathematical modeling of dispersion polymerization of methyl methacrylate in supercritical carbon dioxide. *Ind Eng Chem Res* 42:743–751
43. Mueller PA, Storti G, Morbidelli M (2005) Detailed modeling of MMA dispersion polymerization in supercritical carbon dioxide. *Chem Eng Sci* 60:1911–1925
44. Mueller PA, Storti G, Morbidelli M, Apostolo M, Martin R (2005) Modeling of vinylidene fluoride heterogeneous polymerization in supercritical carbon dioxide. *Macromolecules* 38:7150–7163
45. Wieme J, D'hooge DR, Reyniers MF, Marin GB (2009) Importance of radical transfer in precipitation polymerization of vinyl chloride suspension polymerization. *Macromol React Eng* 3:16–35
46. Mueller PA, Storti G, Morbidelli M, Mantelis CA, Meyer T (2007) Dispersion polymerization of methyl methacrylate in supercritical carbon dioxide: control of molecular weight distribution by adjusting particle surface area. *Macromol Symp* 259:218–225
47. Arosio P, Mosconi M, Storti G, Banaszak B, Hungenberg KD, Morbidelli M (2011) Precipitation copolymerization of vinyl-imidazole and vinyl-pyrrolidone, 2 – kinetic model. *Macromol React Eng* 5:501–517

48. Costa LI, Storti G, Morbidelli M, Ferro L, Galia A, Scialdone O, Filardo G (2012) Copolymerization of VDF and HFP in supercritical carbon dioxide: a robust approach for modeling precipitation and dispersion kinetics. *Macromol React Eng* 6:24–44
49. Paine AJ (1990) Dispersion polymerization of styrene in polar solvents. 7. A simple mechanistic model to predict particle size. *Macromolecules* 23:3109–3117
50. Prochazka O, Stejskal J (1992) Spherical particles obtained by dispersion polymerization: model calculations. *Polymer* 33:3658–3663
51. Shen S, Sudol ED, El-Aasser MS (1994) Dispersion polymerization of methyl methacrylate: mechanism of particle formation. *J Polym Sci A Polym Chem* 32:1087–1100
52. O'Neill ML, Yates MZ, Johnston KP, Smith CD, Wilkinson SP (1998) Dispersion polymerization in supercritical CO₂ with siloxane-based macromonomer. 2. The particle formation regime. *Macromolecules* 31:2848–2856
53. Fehrenbacher U, Ballauff M (2002) Kinetics of the early stage of dispersion polymerization in supercritical CO₂ as monitored by turbidimetry. 2. Particle formation and locus of polymerization. *Macromolecules* 35:3653–3661
54. Cockburn RA, McKenna TFL, Hutchinson RA (2011) A study of particle nucleation in dispersion copolymerization of methyl methacrylate. *Macromol React Eng* 5:404–417
55. Mueller PA, Storti G, Morbidelli M (2005) The reaction locus in supercritical carbon dioxide dispersion polymerization. The case of poly(methyl methacrylate). *Chem Eng Sci* 60:377–397
56. Fehrenbacher U, Muth O, Hirth T, Ballauff M (2000) The kinetics of the early stage of dispersion polymerization in supercritical CO₂ as monitored by turbidimetric measurements, 1. *Macromol Chem Phys* 201:1532–1539
57. Sherwood TK, Pigford RL, Wilke CR (1975) *Mass transfer*. McGraw-Hill, New York
58. McHugh MA, Krukoni VJ (1994) *Supercritical fluid extraction: principles and practice*. Butterworth-Heinemann, Stoneham
59. Bae W, Kwon S, Byun HS, Kim H (2004) Phase behavior of the poly(vinyl pyrrolidone) + N-vinyl-2-pyrrolidone + carbon dioxide system. *J Supercrit Fluids* 30:127–137
60. Wenzel JE, Lanterman HB, Lee S (2005) Experimental *P-T-ρ* measurements of carbon dioxide and 1,1-difluoroethene mixtures. *J Chem Eng Data* 50:774–776
61. Chapman WG, Gubbins KE, Jackson G, Radosz M (1990) New reference equation of state for associating liquids. *Ind Eng Chem Res* 29:1709–1721
62. Müller EA, Gubbins KE (2001) Molecular-based equation of state for associating fluids: a review of SAFT and related approaches. *Ind Eng Chem Res* 40:2193–2211
63. Gupta RB, Prausnitz JM (1995) Vapor-liquid equilibria of copolymer + solvent and homopolymer + solvent binaries: new experimental data and their correlation. *J Chem Eng Data* 40:784–791
64. Simha R, Somcynsky T (1969) On the statistical thermodynamics of spherical and chain molecule fluids. *Macromolecules* 2:342–350
65. Utracki LA, Simha R (2001) Analytical representation of solutions to lattice-hole theory. *Macromol Theory Simul* 10:17–24
66. Sanchez IC, Lacombe RH (1978) Statistical thermodynamics of polymer solutions. *Macromolecules* 11:1145–1156
67. Galia A, Cipollina A, Scialdone O, Filardo G (2008) Investigation of multicomponent sorption in polymers from fluid mixtures at supercritical conditions: the case of the carbon dioxide/vinylidene fluoride/poly(vinylidene fluoride) system. *Macromolecules* 41:1521–1530
68. Cao K, Li BG, Pan ZR (1999) Micron-size uniform poly(methyl methacrylate) particles by dispersion polymerization in polar media. IV. Monomer partition and locus of polymerization. *Colloids Surf A Physicochem Eng Asp* 153:179–187
69. Russell GT, Napper DH, Gilbert RG (1988) Termination in free-radical polymerizing systems at high conversion. *Macromolecules* 21:2133–2140
70. Shen J, Tian Y, Wang G, Yang M (1991) Modelling and kinetic study on radical polymerization of methyl methacrylate in bulk, 1. Propagation and termination rate coefficients and initiation efficiency. *Makromol Chem* 192:2669–2685

71. Achilias DS (2007) A review of modeling of diffusion controlled polymerization reactions. *Macromol Theory Simul* 16:319–347
72. Soh SK, Sundberg DC (1982) Diffusion-controlled vinyl polymerization. II. Limitations on the gel effect. *J Polym Sci Polym Chem Ed* 20:1315–1329
73. North AM (1964) The collision theory of chemical reactions in liquids. Wiley, New York
74. Noyes RM (1961) Effects of diffusion rates on chemical kinetics. In: *Progress in reaction kinetics*, vol 1. Pergamon, New York, pp 131–158
75. Griffiths MC, Strauch J, Monteiro MJ, Gilbert RG (1998) Measurement of diffusion coefficients of oligomeric penetrants in rubbery polymer matrixes. *Macromolecules* 31:7835–7844
76. Masaro L, Zhu XX (1999) Physical models of diffusion for polymer solutions, gels and solids. *Prog Polym Sci* 24:731–775
77. Vrentas JS, Duda JL (1977) Diffusion in polymer-solvent systems. I. Reexamination of the free-volume theory. *J Polym Sci Polym Phys Ed* 15:403–416
78. Zielinski JM, Duda JL (1992) Predicting polymer/solvent diffusion coefficients using free-volume theory. *AIChE J* 38:405–415
79. Vrentas JS, Vrentas CM (1998) Predictive methods for self-diffusion and mutual diffusion coefficients in polymer-solvent systems. *Eur Polym J* 34:797–803
80. Costa LI, Storti G (2010) Self-diffusion of small molecules into rubbery polymers: a lattice free-volume theory. *J Polym Sci B Polym Phys* 48:529–540
81. Kumar SK, Chhabria SP, Reid RC, Suter UW (1987) Solubility of polystyrene in supercritical fluids. *Macromolecules* 20:2550–2557
82. Bonavoglia B, Storti G, Morbidelli M (2006) Modeling the partitioning of oligomers in supercritical CO₂. *Ind Eng Chem Res* 45:3335–3342
83. Arosio P, Mosconi M, Storti G, Morbidelli M (2011) Precipitation copolymerization of vinyl-imidazole and vinyl-pyrrolidone, 1 – experimental analysis. *Macromol React Eng* 5:490–500
84. Chapiro A, Mankowski Z (1988) Polymerisation du vinylimidazole en masse et en solution. *Eur Polym J* 24:1019–1028
85. Chapiro A (1992) Peculiar aspects of the free-radical polymerization of 1-vinylimidazole. *Int J Radiat Appl Instrum C Radiat Phys Chem* 40:89–93
86. Apostolo M, Arcella V, Storti G, Morbidelli M (1999) Kinetics of the emulsion polymerization of vinylidene fluoride and hexafluoropropylene. *Macromolecules* 32:989–1003
87. Galia A, Giaconia A, Scialdone O, Appostolo M, Filardo G (2006) Polymerization of vinylidene fluoride with perfluoropolyether surfactants in supercritical carbon dioxide as dispersing medium. *J Polym Chem A Polym Chem* 44:2406–2418
88. Ahmed TS, DeSimone JM, Roberts GW (2007) Continuous copolymerization of vinylidene fluoride with hexafluoropropylene in supercritical carbon dioxide: low hexafluoropropylene content semicrystalline copolymers. *Macromolecules* 40:9322–9331
89. Darvishi R, Esfahany MS, Bagheri R (2015) S-PVC grain morphology: a review. *Ind Eng Chem Res* 54:10953–10963
90. Smallwood PV (1986) The formation of grains in suspension poly(vinyl chloride). *Polymer* 27:1609–1618
91. Alexopoulos AH, Kiparissides C (2007) On the prediction of internal particle morphology in suspension polymerization of vinyl chloride. Part I: the effect of primary particle size distribution. *Chem Eng Sci* 62:3970–3983
92. Etesami N, Esfahany MN, Bagheri R (2008) Effect of the phase ratio on the particle properties of poly(vinyl chloride) resins produced by suspension polymerization. *J Appl Polym Sci* 110:2748–2755
93. Bao YZ, Brooks BW (2003) Particle features of poly(vinyl chloride) resins prepared by a new heterogeneous polymerization process. *J Appl Polym Sci* 90:954–958
94. Georgiadou S, Thomas NL, Gilbert M, Brooks BW (2009) Nonaqueous polymerization of vinyl chloride: an environmentally friendly process. *J Appl Polym Sci* 112:2472–2481